Li et al. Nanoscale Research Letters (2017) 12:80
DOI 10.1186/s11671-017-1863-9

Nanoscale Research Letters

NANO EXPRESS Open Access

Photocathodic Protection of 304 Stainless Steel by Bi_2S_3/TiO_2 Nanotube Films Under Visible Light

Hong Li[1], Xiutong Wang[1*], Qinyi Wei[1,2] and Baorong Hou[1]

Abstract

We report the preparation of TiO_2 nanotubes coupled with a narrow bandgap semiconductor, i.e., Bi_2S_3, to improve the photocathodic protection property of TiO_2 for metals under visible light. Bi_2S_3/TiO_2 nanotube films were successfully synthesized using the successive ionic layer adsorption and reaction (SILAR) method. The morphology and structure of the composite films were studied by scanning electron microscopy and X-ray diffraction, respectively. UV–visible diffuse reflectance spectra were recorded to analyze the optical absorption property of the composite films. In addition, the influence of Bi_2S_3 deposition cycles on the photoelectrochemical and photocathodic protection properties of the composite films was also studied. Results revealed that the heterostructure comprised crystalline anatase TiO_2 and orthorhombic Bi_2S_3 and exhibited a high visible light response. The photocurrent density of Bi_2S_3/TiO_2 was significantly higher than that of pure TiO_2 under visible light. The sensitization of Bi_2S_3 enhanced the separation efficiency of the photogenerated charges and photocathodic protection properties of TiO_2. The Bi_2S_3/TiO_2 nanotubes prepared by SILAR deposition with 20 cycles exhibited the optimal photogenerated cathodic protection performance on the 304 stainless steel under visible light.

Keywords: TiO_2 nanotube, Bi_2S_3, Stainless steel, Photocathodic protection

Background

304 stainless steel (304SS) is widely used in various industries for its good corrosion resistance and fabricability. However, this material easily deteriorates from pitting corrosion in seawater and chloride-containing solutions [1, 2]. Recently, photocathodic protection for metals has received growing attention from scientists worldwide as a promising and green technology [3–7]. TiO_2 has been extensively investigated as a photoanode for the cathodic protection because of its high chemical stability, low cost, and nontoxicity [8–11]. However, its wide bandgap (~3.2 eV for anatase) restricts its application because of its exclusive activity only under UV irradiation (3–5% of the solar spectrum) [12, 13]. The recombination of photogenerated electrons and holes in the dark results in a low photo-quantum efficiency of TiO_2. To overcome these defects, TiO_2 nanotube arrays with large specific surface areas were synthesized [14–16] and various strategies were developed to expand its absorption to the visible light range. These strategies include coupling with narrow-bandgap semiconductors (ZnSe, WO_3, SnO_2, CdS, and Ag_2S) [17–21], metals (Ag, Au, Cu, and Bi) [22–24], and nonmetals (N, F, and graphene) [25–27]. Bi_2S_3 is an attractive material because of its narrow bandgap ($E_g = 1.3$ eV) and high photo-to-electron conversion efficiency [28]. The Bi_2S_3/TiO_2 heterostructure can reduce the recombination of photogenerated electrons and holes, and this effect would benefit the photoelectric performance of materials [29–32]. However, no research has been reported on the photogenerated cathodic protection property of Bi_2S_3/TiO_2 nanotubes. Successive ionic layer adsorption and reaction (SILAR) is a promising technique with low cost and simple equipment, which can synthesize continuous and compact film at room temperature [33]. In this study, Bi_2S_3/TiO_2 nanotube films served as photoanode for preventing 304SS corrosion. In the fabrication of the films,

* Correspondence: xiutongwang@gmail.com
[1]Key Laboratory of Marine Environmental Corrosion and Bio-fouling, Institute of Oceanology, Chinese Academy of Sciences, No. 7, Nanhai Road, Qingdao 266071, China
Full list of author information is available at the end of the article

Bi_2S_3 nanoparticles were prepared by the SILAR method. The morphology, structure, and optical absorption property were studied by scanning electron microscopy (SEM), X-ray diffraction (XRD), and UV–visible (UV–vis) diffuse reflectance spectra, respectively. The influence of Bi_2S_3 deposition cycles on the photoelectrochemical and photocathodic protection properties of the composite films was also investigated in our work.

Methods

TiO_2 nanotubes were first fabricated by anodizing Ti foil in ethylene glycol electrolyte comprised of 0.5 wt% NH_4F and 6 vol% H_2O for 1.5 h and annealing at 450 °C for 1.5 h in air. Then, Bi_2S_3/TiO_2 nanocomposites were prepared through the alternate immersion of TiO_2/Ti substrate in the anionic and cationic precursor solutions at room temperature. The cationic precursor solution was composed of 0.01 M $Bi(NO_3)_3$ dissolved in 50 ml of acetone. Meanwhile, the anionic precursor solution was composed of 0.01 M Na_2S dissolved in 50 ml of methanol. The TiO_2/Ti substrate was first dipped into the cationic precursor solution for 20 s, and then dipped into the anionic precursor solution for 20 s, rinsed, and dried in air. The Bi_2S_3 synthesized in 10, 20, and 30 deposition cycles were assigned as BST-10, BST-20, and BST-30, respectively.

The morphology of the samples was investigated by SEM (Hitachi S-4800, Japan). The structure of the samples was examined by XRD (Bruker AXSD8 Advance, Germany). The UV–vis diffuse reflectance spectra were obtained on an UV–vis diffuse reflectance spectrophotometer (Hitachi UH4150, Japan). Photoelectrochemical experiments were conducted using a potentiostat/galvanostat (PARSTAT 2273, USA) at room temperature with a Xe lamp (PLS-SXE300C, China) as the visible light source. The open-circuit potential (OCP) of different coupled photoelectrodes were investigated in a double-cell system (Fig. 1a). A TiO_2 or Bi_2S_3/TiO_2 nanotube photoelectrode was placed in a photoanode cell containing a mixed 0.1 M Na_2S and 0.2 M NaOH solution, whereas 304SS was placed in a corrosion cell containing 3.5 wt% NaCl solution. The Pt foil, saturated calomel electrode (SCE), and coupled electrode of TiO_2 and 304SS electrode served as the counter electrode (CE), reference electrode (RE), and working electrode (WE), respectively. Photocurrent curves were measured in 0.2 M Na_2SO_4 solution using an electrochemical workstation (CHI 1010C, China). The TiO_2 or Bi_2S_3/TiO_2 composite photoelectrode, SCE, and Pt foil served as the WE, RE, and CE, respectively (Fig. 1b).

Results and Discussion

The morphologies of Bi_2S_3/TiO_2 heterostructure were observed by SEM (Fig. 2). TiO_2 nanotube arrays exhibited a well-ordered, high-density, and uniform tubular structure with an average diameter of 60 nm (Fig. 2a). The Bi_2S_3 nanoparticles were successfully deposited on TiO_2 nanotube surfaces through the SILAR method (Figs. 2b–d). For BST-10, the particles distributed irregularly on the mouth of TiO_2 nanotubes (Fig. 2b). When the number of Bi_2S_3 deposition cycle increased to 20, the Bi_2S_3 nanoparticles were deposited regularly on the mouth or wall of TiO_2 nanotubes with about 15 nm in diameter. After undergoing 30 cycles, the amount of nanoparticles significantly increased, and the formation of agglomeration caused the particles to block the nanotubes.

Figure 3a depicts the XRD patterns of TiO_2 and Bi_2S_3/TiO_2. Aside from the diffraction peaks of titanium substrate, the peaks at 25.38°, 38.03°, 48.01°, 54.05°, 55.17°, 62.71°, and 70.44° can be indexed to lattice planes (101), (004), (200), (105), (211), (204), and (220) of anatase

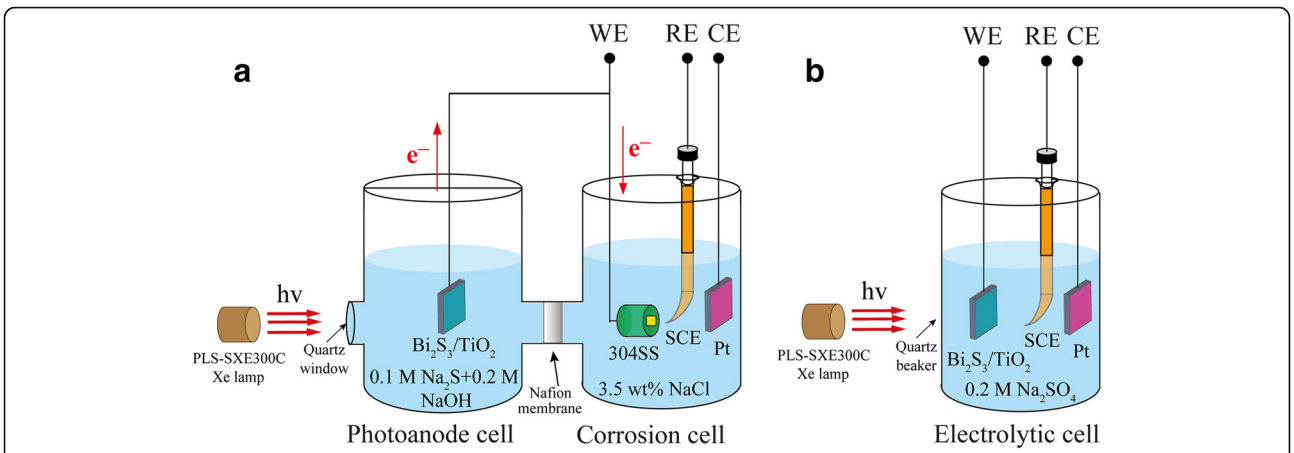

Fig. 1 Schematic sketches of experimental devices for photoelectrochemical characterization of OCPs (**a**) and transient photocurrent curves (**b**)

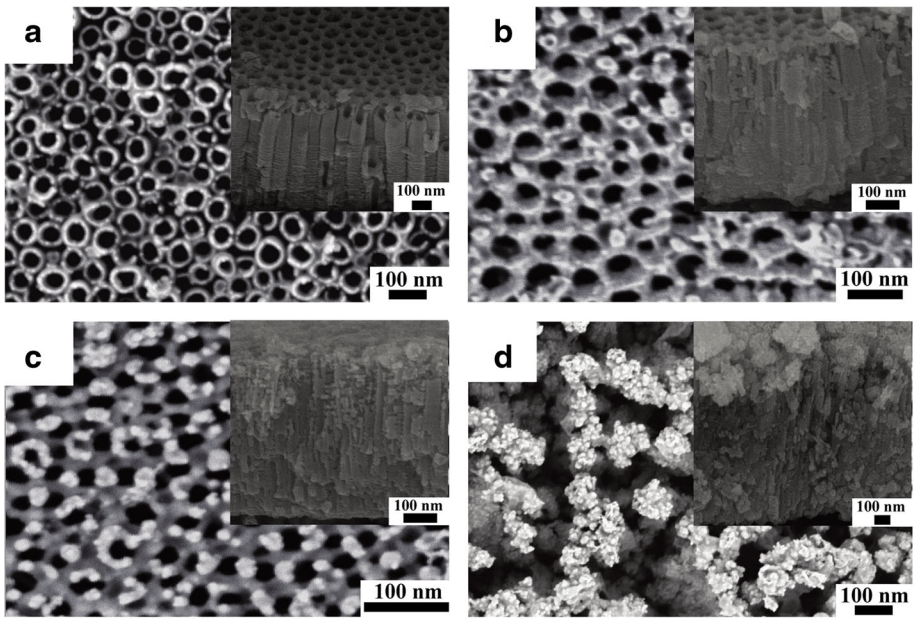

Fig. 2 SEM images of **a** pure TiO_2, **b** BST-10, **c** BST-20, and **d** BST-30

TiO_2, respectively (JCPDS 21-1272). Besides the TiO_2 peaks, the peaks at 27.74° and 32.54° were attributed to lattice planes (211) and (221) of the orthorhombic Bi_2S_3 (JCPDS 17-0320). For Bi_2S_3/TiO_2 nanocomposites, the increase in diffraction peak intensity of Bi_2S_3 with the deposition cycles revealed an increased amount of Bi_2S_3 nanoparticles on the TiO_2 nanotubes. This finding is consistent with the SEM results.

The light absorption abilities of the synthesized Bi_2S_3/TiO_2 nanotube films were assessed by UV–vis spectroscopy (Fig. 3b). Figure 3b shows that TiO_2 nanotubes absorbed mainly in the UV range with a wavelength of about 380 nm because of the bandgap energy of anatase (3.2 eV). The spectra of Bi_2S_3/TiO_2 exhibit a relatively broad and strong absorption in the visible region, indicating that the Bi_2S_3/TiO_2 nanocomposite is capable of harvesting visible light and acts as a photoanode under visible light [34].

Figure 4a displays the transient photocurrent curves for TiO_2 and Bi_2S_3/TiO_2 photoelectrodes under visible light irradiation. The pure TiO_2 nanotube photoelectrode shows nearly 0 $\mu A/cm^2$ because of weak visible light absorption. However, after Bi_2S_3 nanoparticle sensitization, the transient photocurrent densities of

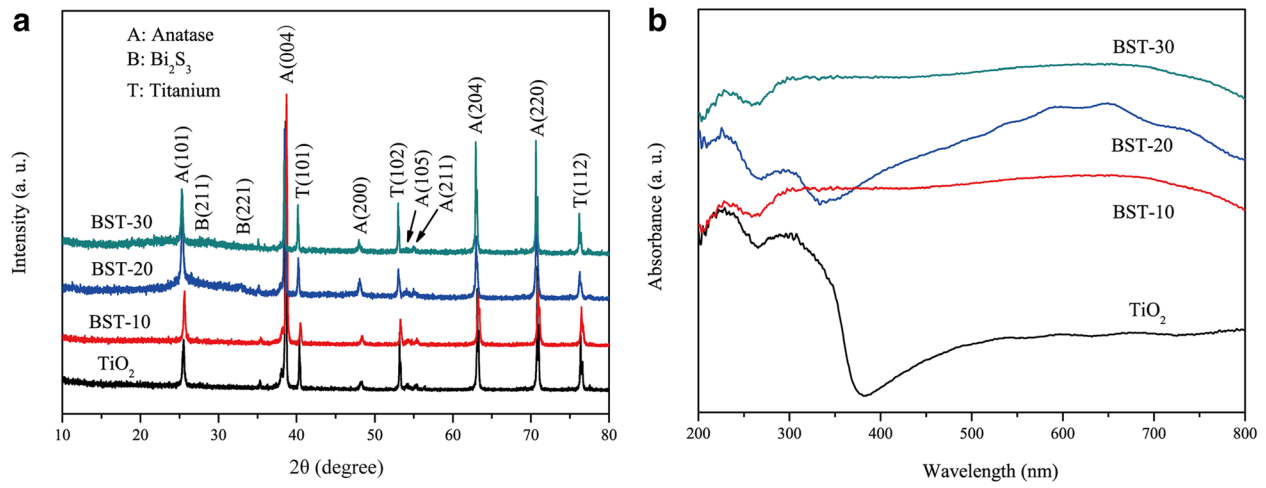

Fig. 3 XRD patterns (**a**) and UV–vis diffuse reflectance spectra (**b**) of pure TiO_2 and Bi_2S_3/TiO_2

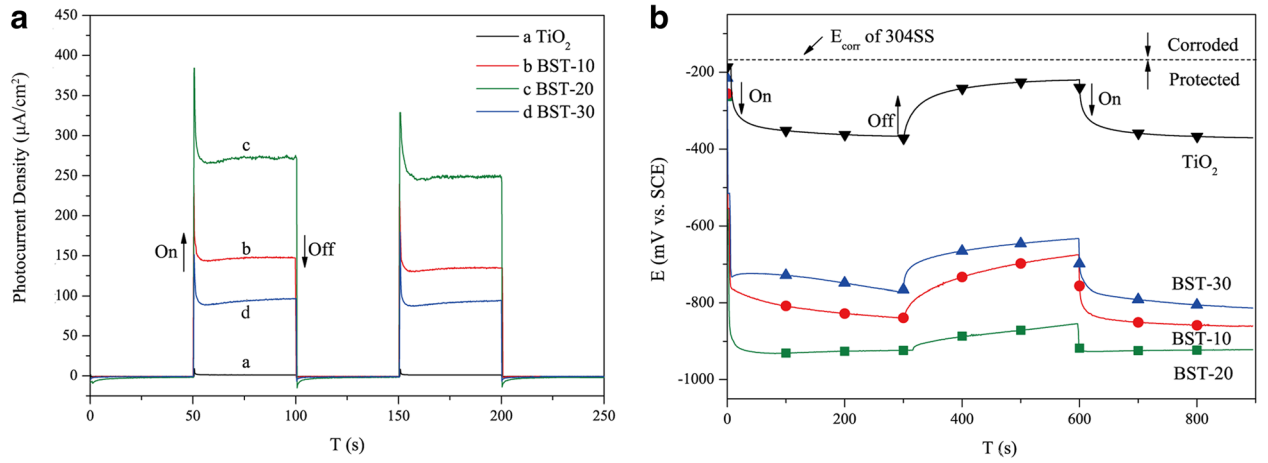

Fig. 4 Photoresponse spectra (**a**) and OCP variations (**b**) of pure TiO_2 and Bi_2S_3/TiO_2 under intermittent irradiation

Bi_2S_3/TiO_2 exhibited an obvious increase, implying that the Bi_2S_3/TiO_2 nanocomposite is capable of utilizing visible light and the heterostructure promotes the separation of photogenerated electrons and holes [35]. The transient photocurrent density of BST-20 (249 μA/cm^2) was higher than that of BST-10 (134 μA/cm^2) and BST-30 (92 μA/cm^2), indicating that BST-20 possesses an optimal separation efficiency of the photogenerated electrons and holes.

Figure 4b compares the photogenerated OCPs of 304SS coupled with different TiO_2 nanotubes. When the light was on, the potentials of coupled electrodes all shifted negatively within a few seconds. This effect may be attributed to the cathodic polarization of 304SS which results from the excited photoelectrons transfer from TiO_2 nanotubes to 304SS [36, 37]. After the light was off, the OCP of 304SS coupled to pure TiO_2 returned to a value near the free corrosion potential of bare 304SS, indicating the invalid recombination of the photogenerated electrons and holes in the TiO_2 [38]. By contrast, the OCPs of 304SS coupled with Bi_2S_3/TiO_2 exhibited a slightly positive shift and stayed far below than the free corrosion potential of bare 304SS. The charges stored in the Bi_2S_3/TiO_2 composite were released and again transferred to 304SS in the dark. The negative shift of potentials is reportedly an important parameter for evaluating the separation efficiency of photogenerated charges [39, 40]. The increased negative shift of the potentials indicates the increased effectiveness of the cathodic protection of photoanodes. Under visible light, the shift of potentials can be ranked in the following order: TiO_2 (150 mV vs. SCE) < BST-30 (534 mV vs. SCE) < BST-10 (572 mV vs. SCE) < BST-20 (662 mV vs. SCE). Hence, BST-20 possesses the optimal photocathodic protection property for 304SS. This result may be due to the fact that the active sites and light harvesting increased with the rising Bi_2S_3 amount. However, the excessive Bi_2S_3 particles served as the recombination sites of the electrons and holes, which hindered the charge transfer from the Bi_2S_3/TiO_2 composite to 304SS.

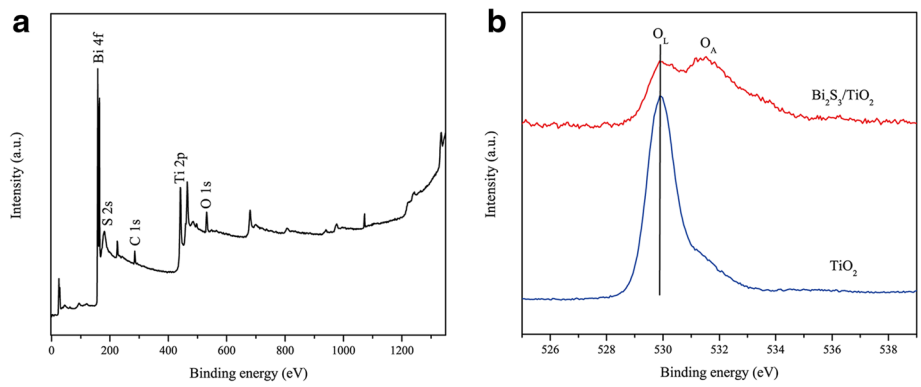

Fig. 5 XPS survey spectra of the synthesized Bi_2S_3/TiO_2 (**a**) and high-resolution XPS spectra of O 1s of TiO_2 and Bi_2S_3/TiO_2 (**b**)

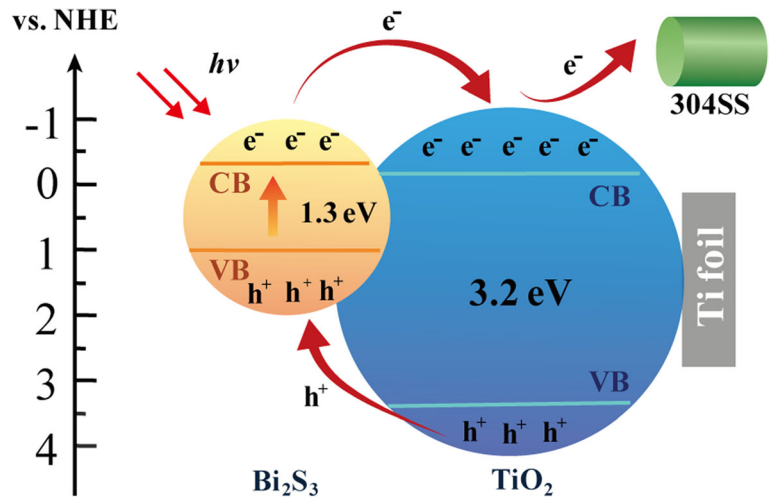

Fig. 6 Schematic representation of the electron transfer processes in Bi_2S_3/TiO_2

The X-ray photoelectron spectroscopy (XPS) was measured to investigate the chemical compositions and states of Bi_2S_3/TiO_2 (BST-20). The XPS survey spectra revealed the existence of Bi, S, Ti, and O components, in addition to C contaminants (Fig. 5a). As shown in Fig. 5b, the XPS peaks of O 1s at 529.7 eV were analyzed from the lattice oxygen (O_L) in TiO_2. The peak at 531.6 eV was derived from the adsorbed oxygen (O_A). The O_A was composed of OH species or weak bonding oxygen on the composite surface. The presence of O_A was ascribed to the generation of oxygen vacancy on the sample surface. This suggests that the Bi_2S_3/TiO_2 composite exhibits higher photocathodic protection properties than TiO_2.

Figure 6 shows the schematic diagram of the photoelectric conversion and transportation processes in the Bi_2S_3/TiO_2 composite. The Bi_2S_3 nanoparticles can easily absorb the photons in the visible light due to the presence of O_A and the suitable bandgap width of Bi_2S_3. When the photons were absorbed by the Bi_2S_3 nanoparticles, the photoexcited electrons were generated and transferred from the conduction band (CB) of Bi_2S_3 to the CB of TiO_2. The photogenerated holes were then shifted from the valence band (VB) of TiO_2 to the VB of Bi_2S_3. When Na_2S served as a hole-trapping agent, the photogenerated charges were effectively separated. The electrons were finally transferred to the 304SS electrode, and the potential of the 304SS electrode negatively shifted. The 304SS was prevented from corrosion by Bi_2S_3/TiO_2 under visible light. Therefore, the more efficient separation of the photogenerated charges in the composite would accelerate the oxidation and reduction reactions and, hence, generate a higher photocathodic protection activity than TiO_2.

Conclusions

In summary, Bi_2S_3-nanoparticle-decorated TiO_2 nanotubes were successfully synthesized through the electrochemical anodization and SILAR method. The sensitization of Bi_2S_3 significantly extended the spectral response from UV to the visible region. Consequently, the composite showed higher photocurrents and cathodic protection performance than pure TiO_2. With increased number of Bi_2S_3 deposition cycles, the increasing grain size and loading of the Bi_2S_3 nanoparticles significantly affected the photocathodic protection activity of the Bi_2S_3/TiO_2 nanocomposite. The Bi_2S_3/TiO_2 nanotubes prepared by SILAR deposition with 20 cycles exhibited the optimal photocathodic protection property.

Abbreviations

304SS: 304 stainless steel; CB: Conduction band; CE: Counter electrode; O_A: Adsorbed oxygen; OCP: Open-circuit potential; O_L: Lattice oxygen; RE: Reference electrode; SCE: Saturated calomel electrode; SEM: Scanning electron microscopy; SILAR: Successive ionic layer adsorption and reaction; VB: Valence band; WE: Working electrode; XRD: X-ray diffraction

Acknowledgements

This work is financially supported by the Shandong Province Postdoctoral Innovation Project (No. 201601001), China Postdoctoral Science Foundation (No. 2015M582150), and CAS Strategic Priority Project (No. XDA13040404).

Authors' Contributions

HL performed the synthesis and characterization of the Bi_2S_3/TiO_2 nanotubes. XW, QW, and BH participated in the characterization. HL supervised the conceptual framework and drafted the manuscript. All authors read and approved the final manuscript.

Competing Interests

The authors declare that they have no competing interests.

Author details

[1]Key Laboratory of Marine Environmental Corrosion and Bio-fouling, Institute of Oceanology, Chinese Academy of Sciences, No. 7, Nanhai Road, Qingdao 266071, China. [2]University of Chinese Academy of Sciences, Beijing 100049, China.

Received: 4 January 2017 Accepted: 24 January 2017
Published online: 31 January 2017

References

1. Zhang Y, Yin XY, Yan FY (2015) Effect of halide concentration on tribocorrosion behaviour of 304SS in artificial seawater. Corros Sci 99:272–80
2. Zhang Y, Yin XY, Yan YF et al (2015) Tribocorrosion behaviors of 304SS: effect of solution pH. RSC Adv 5(23):17676–82
3. Park JH, Park JM (2014) Photo-generated cathodic protection performance of electrophoretically Co-deposited layers of TiO_2 nanoparticles and graphene nanoplatelets on steel substrate. Surf Coat Tech 258:62–71
4. Yuan J, Fujisawa R, Tsujikawa S (1994) Photopotentials of copper coated with TiO_2 by sol-gel method. Zairyo-to-kankyo 43:433–40
5. Yuan J, Tsujikawa S (1995) Characterization of sol-gel-derived TiO_2 coating on carbon steel in alkaline solution. Zairyo-to-kankyo 44:534–42
6. Konishi T, Tsujikawa S (1997) Photo-effect of sol-gel derived TiO_2 coating on type 304 stainless steel. Zairyo-to-kankyo 46:709–16
7. Yuan J, Tsujikawa S (1995) Characterization of sol-gel-derived TiO_2 coatings and their photoeffects on copper substrates. J Electrochem Soc 142:3444–50
8. Subasri R, Shinohara T (2004) Application of the photoeffect in TiO_2 for cathodic protection of copper. Electrochemistry 72(12):880–4
9. Ohko Y, Saitoh S, Tatsuma T et al (2001) Photoelectrochemical anticorrosion and self-cleaning effects of a TiO_2 coating for type 304 stainless steel. J Electrochem Soc 148(1):B24–B28
10. Huang J, Shinohara T, Tsujikawa S (1997) Effects of interfacial iron oxides on corrosion protection of carbon steel by TiO_2 under illumination. Zairyo-to-kankyo 46:651–61
11. Ohko Y, Saitoh S, Tatsuma T et al (2002) Photoelectrochemical anticorrosion and self-cleaning effects of a TiO_2 coating for type 304 stainless steel. Electrochem Solid St 5:B9–B14
12. Thomas AG, Syres KL (2012) Observation of UV-induced Auger features in catechol adsorbed on anatase TiO_2 (101) single crystal surface. Appl Phys Lett 100(171603):1–4
13. Chen Y, Liu KR (2016) Preparation and characterization of nitrogen-doped TiO_2/diatomite integrated photocatalytic pellet for the adsorption-degradation of tetracycline hydrochloride using visible light. Chem Eng J 302:682–96
14. Liu GH, Du K, Wang KY (2016) Surface wettability of TiO_2 nanotube arrays prepared by electrochemical anodization. Appl Surf Sci 388:313–20
15. Wu J, Xu H, Yan W (2016) Photoelectrocatalytic degradation rhodamine B over highly ordered TiO_2 nanotube arrays photoelectrode. Appl Surf Sci 386:1–13
16. Li DG, Chen DR, Wang JD (2016) Effect of acid solution, fluoride ions, anodic potential and time on the microstructure and electronic properties of self-ordered TiO_2 nanotube arrays. Electrochim Acta 207:152–63
17. Zhang L, Wang XT, Liu FG et al (2015) Photogenerated cathodic protection of 304ss by ZnSe/TiO_2 NTs under visible light. Mater Lett 143:116–9
18. Tatsuma T, Saitoh S, Ohko Y et al (2001) TiO_2-WO_3 photoelectrochemical anticorrosion system with an energy storage ability. Chem Mater 13(9):2838–42
19. Subasri R, Shinohara T (2003) Investigations on SnO_2-TiO_2 composite photoelectrodes for corrosion protection. Electrochem Commun 5(10):897–902
20. Bjelajac A, Petrovic R, Socol G et al (2016) CdS quantum dots sensitized TiO_2 nanotubes by matrix assisted pulsed laser evaporation method. Ceram Int 42(7):9011–7
21. Yadav SK, Jeevanandam P (2015) Synthesis of Ag_2S-TiO_2 nanocomposites and their catalytic activity towards rhodamine B photodegradation. J Alloy Compd 649:483–90
22. Fornari AMD, de Araujo MB, Duarte CB et al (2016) Photocatalytic reforming of aqueous formaldehyde with hydrogen generation over TiO_2 nanotubes loaded with Pt or Au nanoparticles. Int J Hydrogen Energ 41(27):11599–607
23. Fu C, Li MJ, Li HJ et al (2017) Fabrication of Au nanoparticle/TiO_2 hybrid films for photoelectrocatalytic degradation of methyl orange. J Alloy Compd 692:727–33
24. Nischk M, Mazierski P, Wei ZS et al (2016) Enhanced photocatalytic, electrochemical and photoelectrochemical properties of TiO_2 nanotubes arrays modified with Cu, Ag Cu and Bi nanoparticles obtained via radiolytic reduction. Appl Surf Sci 387:89–102
25. Zhang DY, Ge CW, Wang JZ et al (2016) Single-layer graphene-TiO_2 nanotubes array heterojunction for ultraviolet photodetector application. Appl Surf Sci 387:1162–8
26. Mazierski P, Nischk M, Golkowska M et al (2016) Photocatalytic activity of nitrogen doped TiO_2 nanotubes prepared by anodic oxidation: the effect of applied voltage, anodization time and amount of nitrogen dopant. Appl Catal B-Environ 196:77–88
27. Samsudin EM, Abd Hamid SB, Juan JC, Basirun WJ, Centi G (2016) Synergetic effects in novel hydrogenated F-doped TiO_2 photocatalysts. Appl Surf Sci 370:380–93
28. Zeng QY, Bai J, Li JH et al (2014) Combined nanostructured Bi_2S_3/TNA photoanode and Pt/SiPVC photocathode for efficient self-biasing photoelectrochemical hydrogen and electricity generation. Nano Energy 9:152–60
29. Yu HJ, Huang J, Zhang H et al (2014) Nanostructure and charge transfer in Bi_2S_3-TiO_2 heterostructures. Nanotechnology 25(21):1–8
30. Peter LM, Wijayantha KGU, Riley DJ et al (2003) Band-edge tuning in self-assembled layers of Bi_2S_3 nanoparticles used to photosensitize nanocrystalline TiO_2. J Phys Chem B 107(33):8378–81
31. Zumeta-Dube I, Ruiz-Ruiz VF, Diaz D et al (2014) TiO_2 sensitization with Bi_2S_3 quantum dots: the inconvenience of sodium ions in the deposition procedure. J Phys Chem C 118(22):11495–504
32. Yang LX, Ding YB, Luo SL et al (2013) Fast growth with crystal splitting of morphology-controllable Bi_2S_3 flowers on TiO_2 nanotube arrays. Semicond Sci Tech 28(3):1–11
33. Wang Y, Chen JY, Jiang LX et al (2016) Photoelectrochemical properties of Bi_2S_3 thin films deposited by successive ionic layer adsorption and reaction (SILAR) method. J Alloy Compd 686:684–92
34. Lu L, Yang D, Liu W et al (2016) In situ solution chemical reaction deposition of Bi_2S_3 quantum dots on mesoscopic TiO_2 films for application in quantum dot sensitised solar cells. Mater Technol 31(3):160–5
35. Liu CJ, Yang Y, Li WZ et al (2016) A novel Bi_2S_3 nanowire @ TiO_2 nanorod heterogeneous nanostructure for photoelectrochemical hydrogen generation. Chem Eng J 302:717–24
36. Lin ZQ, Lai YK, Hu RG (2010) A highly efficient ZnS/CdS@TiO_2 photoelectrode for photogenerated cathodic protection of metals. Electrochim Acta 55(28):8717–23
37. Lei CX, Liu Y, Zhou H et al (2013) Photogenerated cathodic protection of stainless steel by liquid-phase-deposited sodium polyacrylate/TiO_2 hybrid films. Corros Sci 68:214–22
38. Ge SS, Zhang QX, Wang XT et al (2015) Photocathodic protection of 304 stainless steel by MnS/TiO_2 nanotube films under simulated solar light. Surf Coat Tech 283:172–6
39. Li H, Wang XT, Zhang L et al (2015) CdTe and graphene co-sensitized TiO_2 nanotube array photoanodes for protection of 304SS under visible light. Nanotechnology 26(15):155704–804
40. Li J, Lin CJ, Li JT et al (2011) A photoelectrochemical study of CdS modified TiO_2 nanotube arrays as photoanodes for cathodic protection of stainless steel. Thin Solid Films 519(16):5494–502